SVU-International Journal of Engineering Sciences and Applications (2024) 5 (2): 129-139
Print ISSN 2785-9967 | Online ISSN 2735-4571
DOI: 10.21608/SVUSRC.2024.263828.1178

Study of Seismic Response of Mechanically Stabilized Earth Wall

Moamen Abd El Raouf[1,*], and Khaled M. M. Bahloul[2]

Abstract validated finite element analysis was used to study the seismic response of the Mechanically Stabilized Earth (MSE). A series of parametric studies were conducted to investigate the behavior of MSE walls under seismic conditions using finite element analysis. From the numerical analysis, it can be concluded that during the earthquake, in the static case, the axial force in reinforcement decreases as the relative density of the foundation soil increases. Also, in the case of the earthquake, the axial force in reinforcement increases as the relative density of foundation soil increases. Furthermore, in the case of medium and loose sand, the soil acts as a damper to the earthquake motion. Also, the horizontal displacement increases as the relative density of foundation soil increases. Finally, during the earthquake, the horizontal displacement of the MSE wall increases as the groundwater level decreases. Furthermore, the maximum axial force in reinforcement occurred at dry soil conditions. Therefore, the worst case during the earthquake occurred when the groundwater level dropped.

Keywords MSE walls; horizontal displacement; Finite element analysis; Seismic response; Ground water table

1 Introduction

Mechanically Stabilized Earth (MSE) walls have become increasingly popular in recent years. Understanding how MSE walls behave under seismic loading conditions is necessary for reliable design [1– 4]. Numerous field observations show that MSE walls operate satisfactorily compared to rigid walls [5–6].

After the 1995 Kobe earthquake, Tatsuoka et al. [7] evaluated the performance of Tanata retaining walls and found that the MSE wall produced less horizontal displacement than the traditional gravity wall [8]. Due to the friction between soil and reinforcement, the MSE wall is characterized by its excellent deformation under earthquake loads [9–10]. The dynamic response of MSE walls has been studied experimentally using large - scale models [11–12–13], full scale - models [14–15], and reduced- scale models [16–17–18–19]. Moreover, many researchers investigated the behavior of MSE walls under seismic conditions numerically [20–21–22–23]. Okabe [24] created the Mononobe-Okabe method to analyze the stability of retaining walls under earthquake loads.

Hatami and Bathurst [25–26–27] performed numerical analysis on MSE walls that were subjected to varying input ground motions, reinforcement stiffness and reinforcement lengths. They found that these factors had a considerable impact on the reinforcing load and the displacement of the wall during earthquakes, but their effects on the wall's natural frequency were minimal.

Liu H. et al. [28] studied the effect of reinforcement on the seismic response and failure mechanism of MSE walls using numerical analysis. They concluded that failure mechanisms were more intricate than what was anticipated by international codes and guidelines [29]. Moreover, in the case of using a large length of reinforcement, no slip surfaces were generated beyond the reinforced zone. Yu et al. [30] simulated two MSE walls of a bridge near Seattle by finite difference analysis and used Allen and Bathurst's monitored data to

Received: 18 January 2024 / Accepted: 24 April 2024
*Corresponding Author: Moamen Abd El Raouf
moamenabdelmontaleb@azhar.edu.eg
1. Civil Engineering Department, Faculty of Engineering, Al-Azhar University, Qena, Egypt
2. Lecturer, Department of Construction Engineering, October High Institute of Engineering and Technology, Egypt

validate the study's findings [31]. Furthermore, they used two constitutive models, modified Duncan-Chang and Mohr-Coulomb. They found that the Mohr-Coulomb model may be sufficient to simulate the response of a granular backfill under seismic conditions.

Guler and Selek [32] studied the seismic response of the MSE wall using a shaking table test and concluded that reinforcement length and material had an insignificant effect on the dynamic response of the wall. Xie and Leshchinsky [33] studied numerically the effect of reinforcement on the failure mechanism and found that the failure surface extended from the toe of the MSE wall to the farther border of the surcharge. Arman et al. [34] studied the dynamic response of MSE walls using finite element analysis via the OpenSees program. Two different lengths of reinforcement were considered. The response of the MSE wall systems was compared to identical dimensions blocks. They found that the MSE wall with a 6 m long reinforcement acts as a rigid block with no relative displacement. Also, the settlement of the retained soil surface is approximately twice that of the reinforced soil.

Ling et al., [35] developed a numerical method to study the influence of the characteristics of the backfill, vertical spacing between reinforcements, and earthquake motion on the seismic response of MSE walls. They concluded that the lateral displacement of the MSE wall was significantly influenced by the backfill properties and reinforcement arrangement.

In this paper, numerical analysis is performed by the Plaxis program to examine the behavior of the mechanically stabilized earth (MSE) wall during the earthquake. The validated numerical model was used to conduct a series of parametric analyses. The effects of the foundation soil properties and level of groundwater were studied. The wall deformation and axial tensile force in the reinforcing elements were investigated under earthquake loading.

2 Numerical Model Description

Plaxis 2D software was used in this analysis. To verify the accuracy of the numerical model, the physical model by Hatami and Bathurst [36-37] was used. The geometry of the physical model can be defined as shown in Figure (1). Figure 2 shows the geometry of the numerical model used and the finite element output mesh at the end of wall construction (EOC). The numerical model dimensions were chosen to be the same as the experimental model having a height of 3.6m and a width of 6.0 m. The backfill layers are modeled by 15 node elements using the small hardening soil model (HSS).

Medium size mesh was used in the analysis with automatic mesh refinement around structural elements (Bringreve et. al., 2020) [38]. The wall facing elements were modeled using 6 node plate elements. The rigid foundation soil was modeled using the linear elastic model. The geogrids were modeled using geogrid elements with anisotropic properties. The soil–structure interaction was simulated using automatic interface elements between wall-facing, geogrids, and soil layers. The roughness of the interface was chosen to be Rint = 0.75 [39].

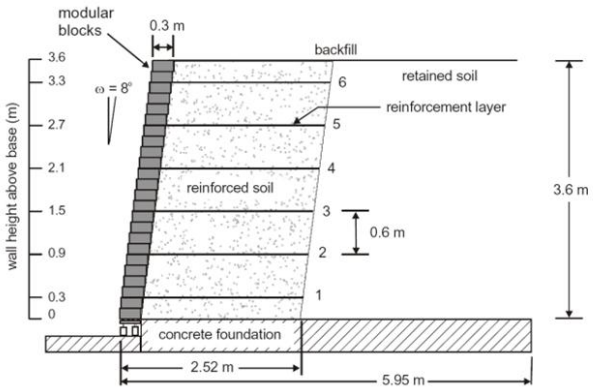

Fig. 1 The geometry of the experimental model (Hatami and Bathurst, 2005)

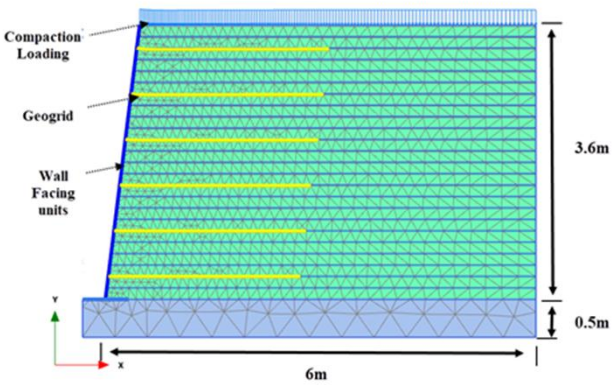

Fig.2 The geometry of the Plaxis 2D model

2.1 Construction of wall simulation

The construction of the wall is simulated using staged construction up to EOC (end of construction) which consists of three steps as follows:

1-Construction of 24 backfill layers of thickness 15cm each layer.
2- Application of a surcharge loading of magnitude 8 kPa at the top of each layer to simulate the compaction process.
3- Installation of six geogrid layers at a spacing of 60cm.

2.2 Material properties

The hardening soil model (Hs) was selected to model the soil layers. This soil model requires the input of 10 parameters as follows: angle of internal friction (ϕ) , soil cohesion (C), dilatancy angle (ψ) , primary oedometer load stiffness (E_{oed}^{ref}), principal load stiffness (E_{50}^{ref}) , failure ratio (R_f), unloading-reloading stiffness (E_{ur}^{ref}) , unloading-reloading Poisson's ratio and finally power m in stiffness laws. These parameters are illustrated in Table (1).

Principal load stiffness $E_{50}^{ref}$is estimated using the following equation:

$$E_{50}^{ref} = \left(\frac{c\cos\phi - \sigma 3 \sin\phi}{c\cos\phi - pref \sin\phi} \right)^{m} \quad (1)$$

Where: c = soil cohesion, ϕ = angle of internal friction, $\sigma'3$ = minor effective principal stress, p_{ref}= reference effective confining stress and m = the degree of stress dependency.

It is recommended to take $E_{ur}^{ref} \sim 3$, E_{50}^{ref} and $E_{oed}^{ref} \sim E_{50}^{ref}$ (Bringreve et. al., 2020) [38].

Table 1. Input parameters used in the analysis [36-37]

Parameter	Value
Backfill - Unit weight γ (kN/m^3)	16.8
MSE wall facing unit weight γ (kN/m^3)	22
E_{50}^{ref} (MPa)	48
E_{oed}^{ref} (MPa)	48
E_{eur}^{ref} (MPa)	144
υ_{ur}	0.2
Angle of Sand internal friction ϕ (°)	44
Cohesion C (kPa)	1
The backfill Dilation angle ψ (°)	11
Power (M) (unitless)	0.5
P_{ref} (kPa)	100
Failure ratio R_f	0.86
R_{int} (unitless)	0.75
Geogrid (EA) (kN/m)	115
Wall Facing E (kPa)	2.0 E+06
Foundation Soil (linear elastic model) E (kPa)	3.0 E+07

3 Validation of the Numerical Model

The results obtained from the numerical model at the end of construction (EOC) indicated that the relative facing displacement began to occur at a depth of 0.083 H (H is the wall height), as shown in Figure (3). Subsequently, the relative facing displacement increased with increasing depth. The maximum relative facing displacement was 6.33 mm and occurred at a depth of 0.67 H. Then the relative displacement decreased with increasing depth. Moreover, the relative displacement at the top of the wall is 3.7 mm.

According to the measured results from the physical model, the relative facing displacement began to occur at a depth of 0.08 H. Also, the maximum displacement was 5.8 mm and happened at a depth of 0.75 H. Then the relative displacement decreased with increasing depth. Furthermore, the relative facing displacement at the top of the wall is 2.5 mm.

It is worth noting that the measured displacement by Hatami and Bathurst represents the magnitude of the facing unit displacement from the time of placement of the facing unit to the end of construction. The relative facing displacement should not be confused with the actual total displacement of the wall at the end of construction and applying the surcharge loading [36]. The same applies to the results of the numerical analysis. Accordingly, the results obtained from the numerical model are in good agreement with the measured results by Hatami and Bathurst as shown in figure (3).

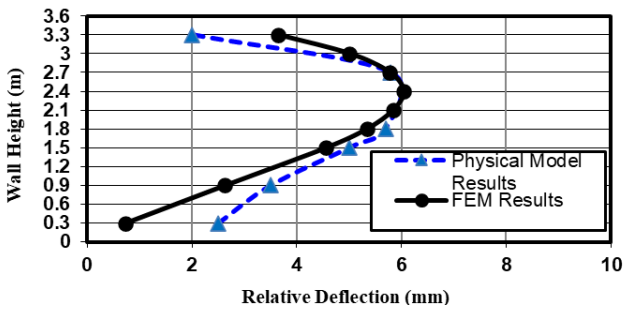

Fig.3 The physical model results at EOC versus FEM results

4 Dynamic Analysis

Dynamic analysis is performed to simulate the effect of a 5.4 Richter magnitude earthquake (Mw = 5.4) on the performance of the MSE wall. The maximum peak ground acceleration (PGA) of 0.24g was used, which is equivalent to the typical expected earthquake intensity in Egypt. The earthquake duration is 23 seconds. Figure (4) shows the input file used in dynamic analysis [38].

Dynamic input is applied at the bottom of the model. As shown in Figure (5) prescribed displacement was imposed in the horizontal direction to prevent vertical direction movement, and standard earthquake fixity was

applied to the model where absorbent boundaries are applied to absorb waves at the external limit of the model.

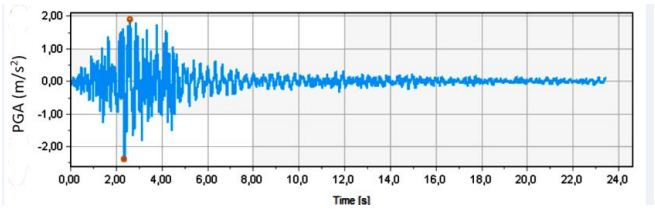

Fig.4 Acceleration (m/s^2) Vs Time

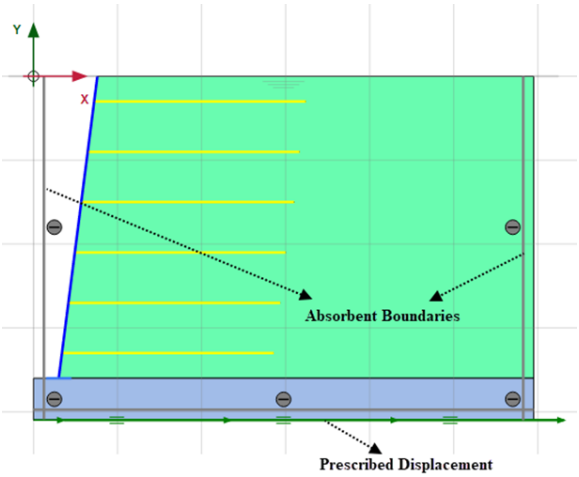

Fig. 5 Dynamic Analysis model setup

4.1 MSE Wall Natural Frequency

The MSE wall natural or fundamental frequency ($f_{11}{}^{R}$) was estimated using an empirical formula based on wall height (H) proposed by Richardson (1978) [40] as follows:

$(f_{11}{}^{R}) = 38.1/H$ (2)

Therefore, the natural frequency of MSE wall = 10.58 Hz.

4.2 Estimating Damping

damping parameters of Rayleigh α and β are estimated using target frequencies. Since the natural frequency of the MSE wall was 10.58 Hz, the range of frequencies used in the analysis was selected to be f_1= 2 Hz andf_2=12 Hz corresponding to the input motion file and natural frequency of the MSE wall. The following equations (Bringreve et. al., 2020) [38] are used to estimate Rayleigh α and β.

$$a = 2\omega_1\omega_2\frac{\omega_1\xi_2 - \omega_2\xi_1}{\omega_1{}^2 - \omega_2{}^2} \quad and \quad \beta = 2\frac{\omega_1\xi_1 - \omega_2\xi_2}{\omega_1^2 - \omega_2^2} \qquad (3)$$

where: ω = Angular velocities = 2πf, ζ= Target damping ratio chosen to be 10% as recommended by (Moradi, 2014) [41] for MSE walls.

Using equation (3) α=2.154, β= 0.002274

Rayleigh α and β values are defined for facing units, soil backfill and foundation soil and no specific damping ratio is assigned to the geogrid.

5 Dynamic Response of MSE Wall

In this section, the MSE wall behavior was studied in static and seismic conditions. After the static analysis of the MSE wall, the dynamic analysis is executed, and the displacement is reset to zero. The dynamic analysis is considered the last stage of construction.

In the static case, the maximum horizontal displacement was 16.72 mm and occurred at the upper portion of the wall. This is because the vertical pressure increases towards the bottom of the MSE wall. Moreover, the horizontal displacement at the lower portion of the MSE wall was 7.27mm.

During the earthquake, the maximum horizontal displacement was -19.17 mm and occurred at the lower portion of the MSE wall. Furthermore, the horizontal displacement at the upper portion of the wall was -10.11 mm, as shown in Figure (6). Also, it can be noticed that the lower portion of the wall is the most affected by the earthquake. This is due to that the lower portion of the wall is the closest part of the wall to the ground motion. Moreover, during the earthquake, the horizontal displacement occurred in a direction opposite to the static condition.

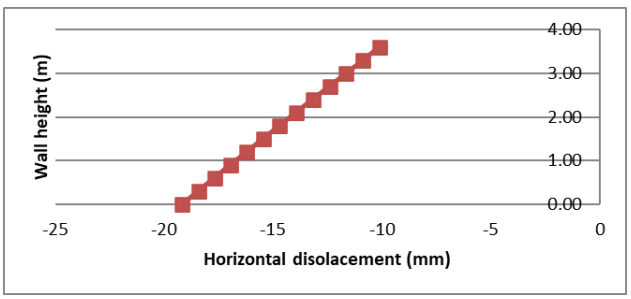

Fig. 6 Wall horizontal displacement versus the wall height during earthquake

From Figures (7.a) to (7.f) it can be noticed that the earthquake caused an increase in axial force for the geogrid layers (6, 5, 4, 3, 2 and 1) by 274% 155%, 135%, 162%, 234% and 201% respectively. The axial tensile force in the reinforcement layers increased significantly during the earthquake. The maximum increase was 274%.

Therefore, a reduction factor equal to 3.0 must be taken into consideration when calculating the allowable tensile strength of the geogrid to resist the earthquake loading.

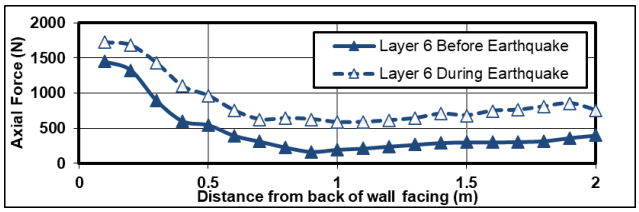

Fig. (7. a) Effect of the earthquake on the axial force of the reinforcement

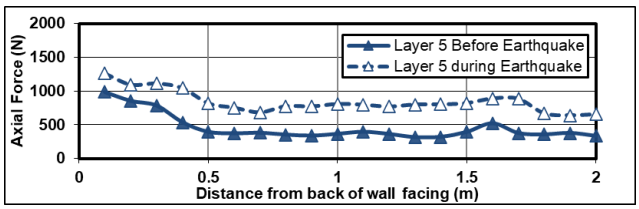

Fig. (7. b) Effect of the earthquake on the axial force of the reinforcement

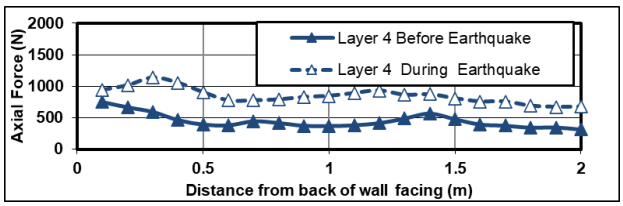

Fig. (7. c) Effect of the earthquake on the axial force of the reinforcement

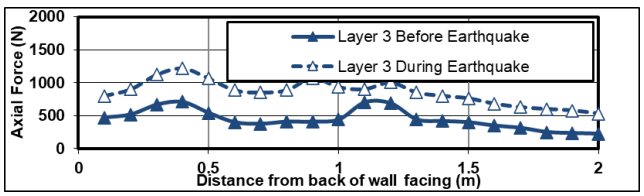

Fig. (7. d) Effect of the earthquake on the axial force of the reinforcement

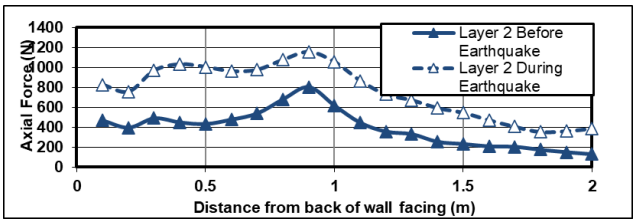

Fig. (7. e) Effect of the earthquake on the axial force of the reinforcement

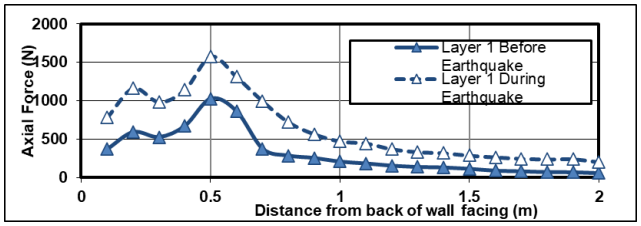

Fig. (7. f) Effect of the earthquake on the axial force of the reinforcement

6 Parametric Study

In this section, the effect of the desired parameters was studied in both static and seismic conditions. In the parametric study, all parameters are held constant except the parameter under study.

6.1 Effect of foundation soil

In this section, different types of foundation soil (loose sand with Dr=30%, medium sand with Dr=50% and dense sand with Dr=75%) were considered, where (Dr) is the relative density. The input parameters used in the analysis of foundation soils are shown in Table (2).

Table (2) Input parameters used in PLAXIS 2D for foundation soils

Parameter	Relative Density (Dr)		
	30%	50%	70%
Unit weight (kN/m^3)	16	17	18
Modulus of elasticity E50^{ref} (MPa)	25	35	50
E50oed^{ref} (MPa)	25	35	50
E50ur^{ref} (MPa)	75	105	150
Poisson ratio (μ)	0.2	0.2	0.2
Angle of internal friction (ϕ°)	31°	33°	36°
Cohesion c (kN/m^2)	1	1	1
Dilatancy angle (Ψ°)	1°	3°	6°
Failure ratio (R_f)	0.9	0.9	0.9
Power (M) (unit less)	0.5	0.5	0.5

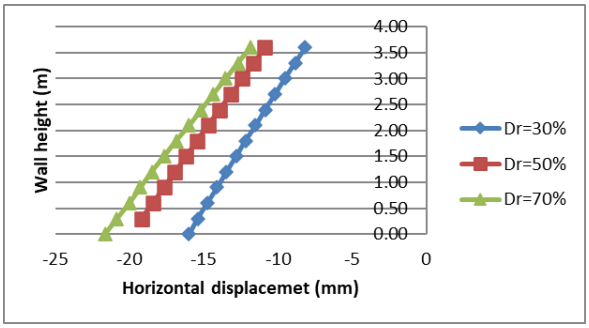

Fig.8 Wall horizontal displacement versus the wall height during earthquake

From Figure (8) it can be noticed that the maximum horizontal displacement during the earthquake was -21.85,-19.17 and -15.4 mm at Dr= 70%, Dr=50% and Dr= 30% respectively. Furthermore, the maximum horizontal displacement during the earthquake occurred at the lower portion of the wall. This is due to that the lower portion of the wall is the closest part of the wall to the ground motion.

It can clearly be distinguished that the horizontal displacement increases as the relative density of foundation soil increases. This is due to the medium and loose soil acting as a damper for the earthquake. But acceleration was amplified in the case of dense sand.

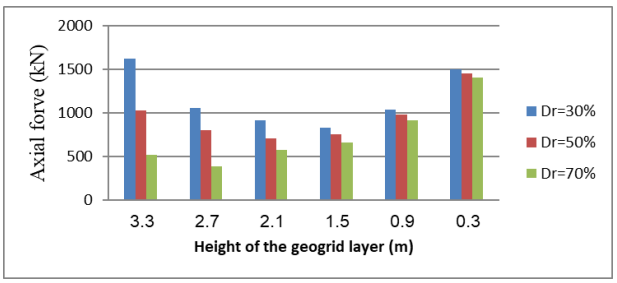

Fig.9 The axial force in reinforcement in static case

Moreover, in the static case, the axial force in reinforcement decreases as the relative density of the foundation soil increases, as shown in Figure (9). This is because the settlement of the foundation soil is greater in loose and medium soil. Increasing the settlement of the foundation soil leads to an increase in axial force in the reinforcement.

The exact opposite happened in the case of the earthquake. The results of the numerical analysis revealed that during the earthquake, the axial force in reinforcement increased as the relative density of foundation soil increased, as shown in Figure (10).

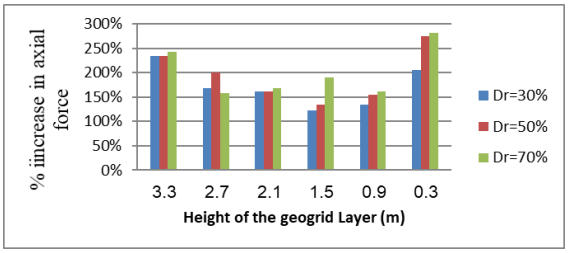

Fig. 10 The increase in axial force in reinforcement during earthquake

This phenomenon can be explained as follows: in the case of medium and loose sand, the shear stress increases with the increase in horizontal displacement resulting from the earthquake. The reason for this is that the void ratio in the loose soil decreases with an increase in the shear stress resulting from the earthquake, and compaction of the soil occurs.

In dense sand, there are few voids in the soil, and the shear stress resulting from the earthquake increases, which causes compaction of the soil. Afterwards, as the shear stress increases, the soil particles slide over each other, which leads to a gradual increase in the void ratio, and the soil turns into a loose state, as shown in Figure (11)[42].

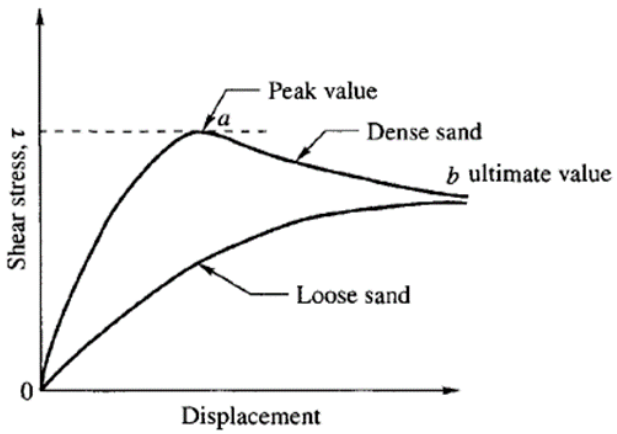

Fig. 11 Shear stress versus displacement for loose and dense sands [42]

From Figures (12. a) to (12. f) it can be noticed that the largest increase in axial force for loose soil was in Geogrid No. 1, which is close to the foundation soil, as a result of the soil volumetric changes due to the earthquake. Furthermore, the largest increase in axial force as a result of the earthquake was for the medium and dense soil in the highest layer (Geogrid No. 6).

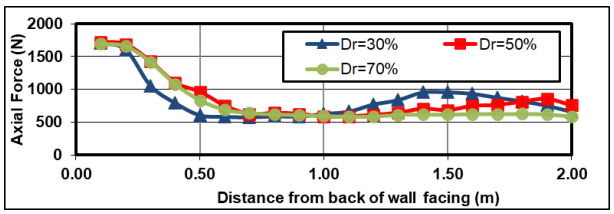

Fig. (12. a) Effect of the earthquake on the axial force (Layer 6)

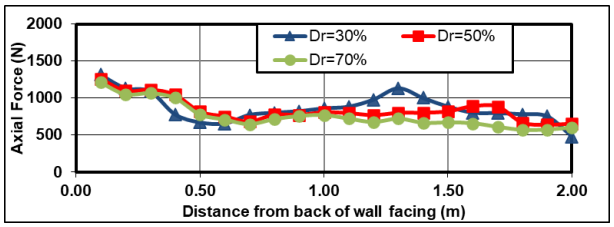

Fig. (12. b) Effect of the earthquake on the axial force (Layer 5)

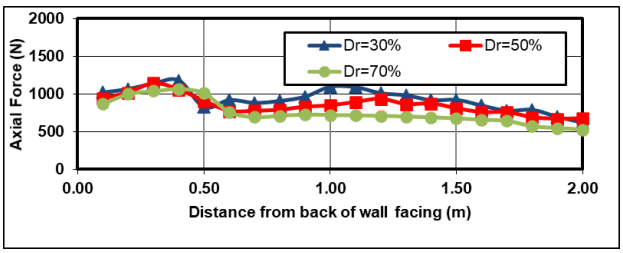

Fig. (12. c) Effect of the earthquake on the axial force (Layer 4)

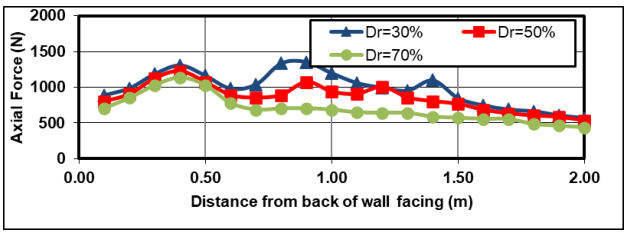

Fig. (12. d) Effect of the earthquake on the axial force (Layer 3)

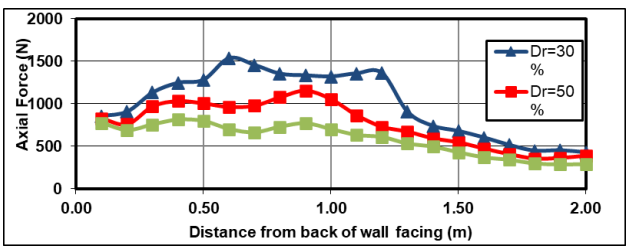

Fig. (12. e) Effect of the earthquake on the axial force (Layer 2)

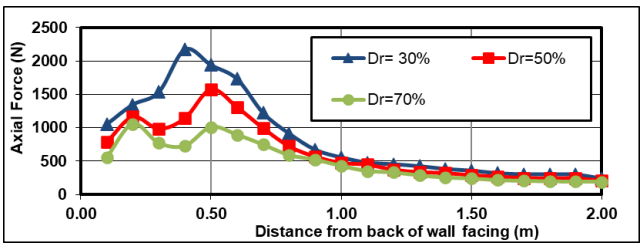

Fig. (12. f) Effect of the earthquake on the axial force (Layer 1)

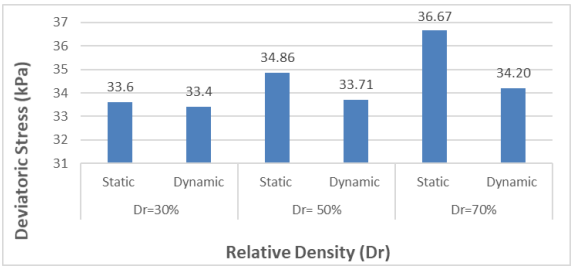

Fig.13 The deviator stress below the wall in static case and dynamic case

From Figure (13), it can be seen that in the case of loose sand, the deviator stress before and during the earthquake is almost the same. Furthermore, the value of the increase in deviator stress in the case of dense soil was greater than the increase in the case of medium soil. In other words, as the relative density of the foundation soil increases, the deviator stress below the wall increases.

6.2 Effect of Groundwater Level

To investigate the influence of groundwater level changes, a numerical analysis was conducted to determine the effect of the ratio D/B on the seismic response of the MSE wall. Where (D) is the depth of groundwater from the ground surface and (B) is the width of MSE at the base.

Figure (14) shows the influence of the groundwater level on the horizontal displacement of the MSE wall and the comparison with the dry case during the earthquake.

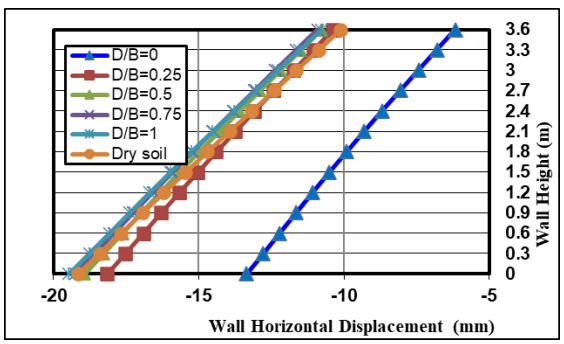

Fig.14 Influence of groundwater level on the horizontal displacement during the earthquake

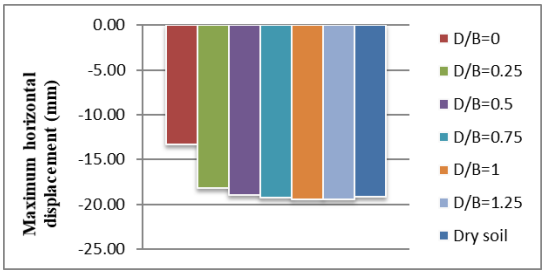

Fig.15 The relation between the maximum horizontal displacement and the groundwater level

As shown in Figures (14) and (15), in the dry condition, the maximum horizontal displacement during the earthquake was -19.17.

In wet conditions, the maximum horizontal displacement during the earthquake was -13.35, -18.94, -19.26, and -19.48 mm for D/B = 0, 0.25, 0.5, 0.75, and 1.0, respectively.

According to the numerical results, it can be noticed that the horizontal displacement of the MSE wall increases as the groundwater level decreases. Furthermore, for D/B >1.0, there is no effect of changing the groundwater level. This means the effect of the water table disappears when the water table is at a depth (D) equal to the width of the MSE wall (B). This phenomenon can be explained as follows: if saturated sandy soil is subjected to shear stresses resulting from an earthquake and the void ratio is higher than the critical void ratio, excess pore-water pressure will be generated due to the soil compressibility and the short time of occurrence of the shear, as shown in Figure 16. When excess pore-water pressure is generated, the effective pressure decreases, and vice versa. Therefore, the worst case during the earthquake occurred when the groundwater level dropped. From the previous analysis, it can be observed that the importance of the groundwater level on the behavior of the MSE wall during the earthquake.

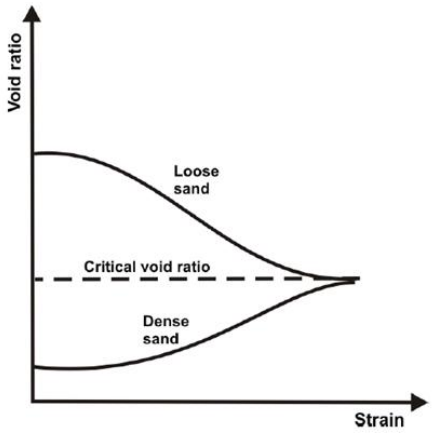

Fig. 16 The critical void ratio [42]

As shown in Figures (17. a) to (17. f) for geogrid layer 6, the maximum axial force in the reinforcement during the earthquake decreased by about 19% for D/B =0.25, 0.5, 0.75 and, 1.0. For D/B=0, the maximum axial force in the reinforcement decreased by about 11%.

For geogrid layer 5, the maximum axial force in the reinforcement during the earthquake increased by about 11% % for D/B =0.25, 0.5, 0.75, and 1.0. For D/B=0, the maximum axial force in the reinforcement increased by about 20%.

For geogrid layer 4, the maximum axial force in the reinforcement during the earthquake increased by about 8% % for D/B =0.25, 0.5, 0.75, and 1.0. For D/B=0, the maximum axial force in the reinforcement increased by about 22%.

For geogrid layer 3, the maximum axial force in the reinforcement during the earthquake decreased by about 20% % for D/B =0.25, 0.5, 0.75 and, 1.0. For D/B=0, the maximum axial force in the reinforcement increased by about 8%.

For geogrid layer 2, the maximum axial force in the reinforcement during the earthquake decreased by about 26% % for D/B =0.25, 0.5, 0.75, and 1.0. For D/B=0, the maximum axial force in the reinforcement decreased by about 19%.

For geogrid layer 1, the maximum axial force in the reinforcement during the earthquake decreased by about 30% % for D/B =0.25, 0.5, 0.75, and 1.0. For D/B=0, the maximum axial force in the reinforcement increased by about 23%.

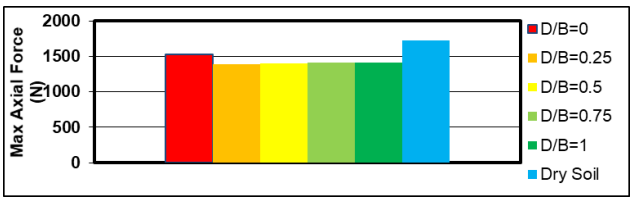

Fig. (17.a) The relation between the maximum axial force in reinforcement and the groundwater level (Layer 6)

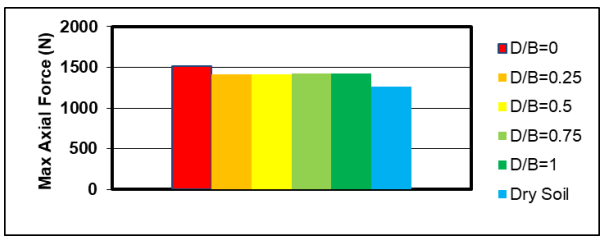

Fig. (17.b) The relation between the maximum axial force in reinforcement and the groundwater level (Layer 5)

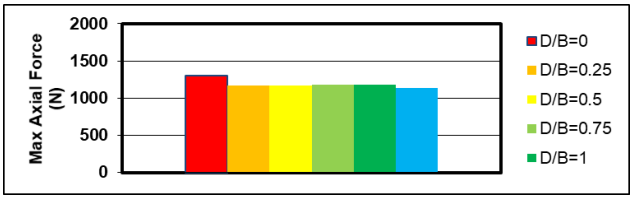

Fig. (17.c) The relation between the maximum axial force in reinforcement and the groundwater level (Layer 4)

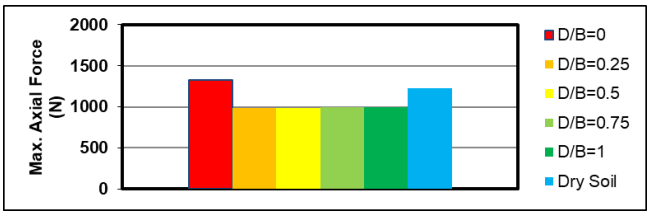

Fig. (17.d) The relation between the maximum axial force in reinforcement and the groundwater level (Layer 3)

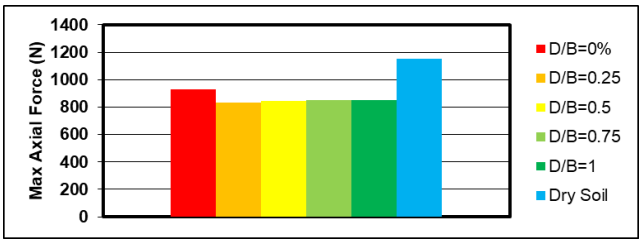

Fig. (17.e) The relation between the maximum axial force in reinforcement and the groundwater level (Layer 2)

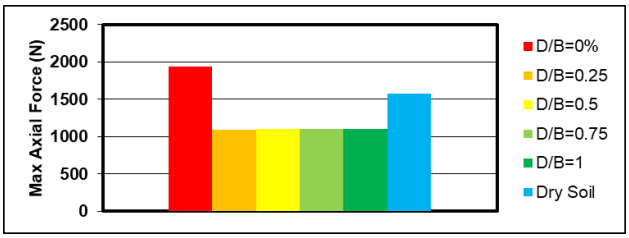

Fig. (17.f) The relation between the maximum axial force in reinforcement and the groundwater level (Layer1)

According to the previous analysis, the maximum axial force in reinforcement during the earthquake occurred at dry soil conditions and D/B=0.

Generally, when D/B =0.25, 0.5, 0.75, and 1.0, the same effect occurs. However, the effect is different when D/B = 0 because the deviator stress below the MSE wall when D/B =0.25, 0.5, 0.75, and 1.0 is nearly the same as shown in Figure 18.

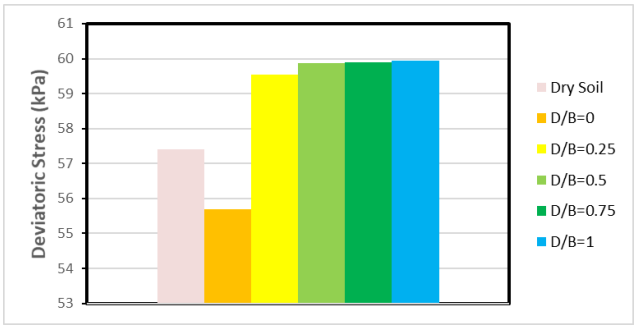

Fig.18 The deviator stress under the MSE wall

7 Conclusions and Recommendations

From the results of the analysis, the following conclusions can be drawn:

- It's recommended to take a reduction factor equal to 3.0 when calculating the allowable tensile strength of the geogrid to resist the earthquake loading.

- In the static case, the axial force in reinforcement decreases as the relative density of the foundation soil increases. This is because the settlement of the foundation soil is greater in loose and medium soil. Increasing the settlement of the foundation soil leads to an increase in axial force in the reinforcement.

- In the case of the earthquake, the axial force in reinforcement increases as the relative density of foundation soil increases.

- The soil type affects significantly the amplification of acceleration. In the case of medium and loose sand, the soil acts as a damper to the earthquake motion. Also, the horizontal displacement increases as the relative density of foundation soil increases.

- During the earthquake, as the relative density of the foundation soil increases, the deviator stress below the wall increases.

- During the earthquake, the horizontal displacement of the MSE wall increases as the groundwater level decreases. Furthermore, the maximum axial force in reinforcement occurred at dry soil conditions. Therefore, the worst case during the earthquake occurred when the groundwater level dropped.

References

[1] Allen T M, Bathurst R J. Performance of an 11 m high block-faced geogrid wall designed using the K-stiffness method. Canadian Geotechnical Journal, 51(1): 16−29 (2014)

[2] Stuedlein A W, Bailey M, Lindquist D, Sankey J, Neely W J. Design and performance of a 46-m-high MSE wall. Journal of Geotechnical and Geoenvironmental Engineering, 136(6): 786−796 (2010)

[3] Jiang Y, Han J, Parsons R L, Brennan J J. Field instrumentation and evaluation of modular-block MSE walls with secondary geogrid layers. Journal of Geotechnical and Geo environmental Engineering, 142(12): 05016002(2016)

[4] Abd El Raouf, M. compaction–Induced Stress In Geosynthetic Reinforced Soil Walls, JES. Journal of Engineering Sciences, 47(No 4), pp. 451-460. (2019) doi: 10.21608/JESAUN.2019.109854

[5] Shishegaran A, Khalili M R, Karami B, Rabczuk T, Shishegaran A. , Computational predictions for estimating the maximum deflection of reinforced concrete panels subjected to the blast load. International Journal of Impact Engineering139: 103527 (2020)

[6] Shishegaran A, Ghasemi M R, Varaee H. Performance of a novel bent-up bars system not interacting with concrete. Frontiers of Structural and Civil Engineering, 13(6): 1301−1315 (2019)

[7]Tatsuoka F, Tateyama M, Mohri Y, Matsushima K. Remedial treatment of soil structures using geosynthetic-reinforcing technology. Geotextiles and Geomembranes, 25(4–5): 204−220 (2007)

[8] Zhang, F., Zhu, Y., Chen, Y. et al. Seismic effects on reinforcement load and lateral deformation of geosynthetic-reinforced soil walls. Front. Struct. Civ. Eng. 15, 1001–1015 (2021). https://doi.org/10.1007/s11709-021-0734-8

[9] Cai Z, Bathurst RJ Seismic-induced permanent displacement of geosynthetic-reinforced segmental retaining walls. Can Geotech J 33(6):937–955. https://doi.org/10.1139/t96-123(1996)

[10] Chen, Y.; Zhao, W.; Jia, P.J.; Han, J.Y.; Guan, Y.P. Dynamic behavior of an embedded foundation under horizontal vibration in a poroelastic half-Space. Appl. Sci. 9, 740 (2019)

[11] Bathurst, R.J., Walters, D., Vlachopoulos, N., Burgess, P., Allen, T.M.,
. Full scale testing of geosynthetic reinforced walls. Geotech. Geoenviron. Eng. 291 (14), 201–217 (2000)

[12] Ling, H.I., Mohri, I., Leshchinsky, D., Burke, C., Matsushima, K., Liu, H. Large-scale shaking table tests on modular-block reinforced soil retaining walls. Geotech. Geoenviron. Eng. 131 (4), 465–476 (2005)

[13] Wang, L., Chen, G., Chen, S., Experimental study on seismic response of geogrid reinforced rigid retaining walls with saturated backfill sand. Geotext. Geomembr. 43 (1), 35–45(2015)

[14] Richardson, G.N., Feger, A., Lee, K.L. Seismic testing of reinforced earth walls. Geotech. Geoenviron. Eng. 103 (1), 1–17(1977)

[15] Futaki, M., Ogawa, N., Sato, M., Kumada, T., Natsume, S. Experiments about seismic performance of reinforced earth retaining wall. In: Proceedings of the 11th World Conference on Earthquake Engineering, Paper no. 1083(1966)

[16] Koseki, J., Tatsuoka, F., Watanabe, K., Tateyama, M., Kojima, K., Munaf, Y. Model tests of seismic stability of several types of soil retaining walls. In: Ling, H., Leshchinsky, D., Tatsuoka, F. (Eds.), Reinforced Soil Engineering Advances in Research and Practice. Marcel Dekker, New York, pp. 378–385 (2003)

[17] El-Emam, M.M., Bathurst, R.J. Influence of reinforcement parameters on the seismic response of reduced-scale reinforced soil retaining walls. Geotext. Geomembr. 25 (1), 33–49(2007)

[18] Ling, H.I., Leshchinsky, D., Wang, J.P., Mohri, Y., Rosen, A. Seismic response of geocell retaining walls: experimental studies. Geotech. Geoenviron. Eng. 135 (4), 515–524(2009)

[19] Huang, C. C., Horng, J.-C., Chang, W. J., Chiou, J. S., Chen, C. H. Dynamic behavior of reinforced walls - horizontal displacement response. Geotext. Geomembr. 29, 257–267(2011)

[20] Jean B. P., Alain C. Emmanuel Bourgeois. Dynamic behavior of a Mechanically Stabilized Earth wall under harmonic loading: Experimental characterization and 3Dfinite elements model. Computers and Geotechnics, Elsevier 65, pp.199-211(2015)

[21] Latha GM, Krishna AM (2008) Seismic response of reinforced soil retaining wall models: influence of backfill relative density. Geotext Geomembr 26(4):335–349(2015) https://doi.org/10.1016/j.geotexmem.2007.11.001

[22] Varnier JB, Hatami K. Seismic response of reinforced soil retaining walls: is PGA-based design adequate? In: Geo-risk 2011: risk assessment and management .p. 336–43(2011)

[23] Xu, P., Zhong, Y., Hatami, K., Yang, G., Liu, W., & Jiang, G. Influence of reinforcement design on seismic stability of full-height panel MSE walls. Soil Dynamics and Earthquake Engineering, 165, 107674 (2023). https://doi.org/10.1016/j.soildyn.2022.107674

[24] Okabe, S. General theory on earth pressure and seismic stability of retaining wall and dam. J. Jpn. Soc. Civ. Eng. 10, 1277–1323(1924)

[25] Hatami K, Bathurst RJ. Investigation of seismic response of reinforced-soil retaining walls. In: 4th international conference on recent advances in geotechnical earthquake engineering and soil dynamics, San Diego, CA, USA, Paper no. 7.18(2001)

[26] Hatami K, Bathurst RJ. Effect of structural design on fundamental frequency of reinforced-soil retaining walls. Soil Dynam Earthq Eng. 19(3):137–57(2000)

[27] Hatami, K., R. J. Bathurst and M. M. El-Emam, 2005. Acceleration amplification in the backfill ofreinforced soil walls with different heights. 3rd Biot Conference on poromechanics, Norman,Oklahoma, USA (Abousleiman, Cheng & Ulm Eds.), Balkema, London, 725-731 (2005)

[28] Liu H, Wang X, Song E. Reinforcement load and deformation mode of geosynthetic-reinforced soil walls subject to seismic loading during service life. Geotext Geomembranes; 29 (1):1–16 (2011)

[29] Berg RR, Christopher BR, Samtani NC. Design and construction of mechanically stabilized earth walls and reinforced soil slopes, 1. Washington, DC, USA: Federal Highway Administration; Publication No. FHWA-NHI-10-024(2009)

[30] Yu, Y., Bathurst, R.J., Allen, T.M., Numerical modeling of the SR-18 geogrid reinforced modular block retaining walls, 142 (5) (2016) https://doi.org/10.1061/(ASCE) GT.1943-5606.0001438.

[31] Allen, T.M., Bathurst, R.J. Performance of an 11 m high block-faced geogrid wall designed using the K-stiffness method. Can. Geotech. J. 51 (1), 16–29(2014) https://doi. org/10.1139/cgj-2013-0261.

[32] Guler E, Selek O. Reduced-scale shaking table tests on geosynthetic-reinforced soil walls with modular facing. J Geotech Geoenviron Eng 140(6):04014015(2014)

[33] Xie, Y., Leshchinsky, B. MSE walls as bridge abutments: optimal reinforcement density. Geotext. Geomembranes 43 (2), 128–138 (2015) https://doi.org/10.1016/j. geotexmem.2015.01.002.

[34] Kamalzadeh, A., & Pender, M. J. Dynamic response of Mechanically Stabilised Earth (MSE) structures: A numerical study. Geotextiles and Geomembranes, 51(1), 73-87 (2023) https://doi.org/10.1016/j.geotexmem.2022.09.008

[35]Ling, H. I., Liu, H., & Mohri, Y. Parametric Studies on the Behavior of Reinforced Soil Retaining Walls under Earthquake Loading. Journal of Engineering Mechanics, 131(10), 1056 1065(2005)
doi:10.1061/(ASCE)0733-9399(2005)131:10(1056)

[36] Hatami, K. and Bathurst, R. J. Development and verification of a numerical model for the analysis of geo-synthetic-reinforced soil segmental walls under working stress conditions. Canadian Geotechnical Journal 42(4):1066-1085 (2005).

[37] Hatami K. and Bathurst R. J. Numerical Model for Reinforced Soil Segmental Walls under Surcharge Loading. Journal of Geotechnical and Geoenvironental Engineering, ASCE, 132(6), 673-684(2006)

[38] BRINKGREVE, R. B. J. PLAXIS 2D Manual, Delft (2020)

[39] Brinkgreve, R. B. J. PLAXIS 2D Version 8 Reference Manual, Delft University of Technology and PLAXIS bv The Netherlands(1998)

[40] Richardson, G. N. Earthquake Resistant Reinforced Earth Walls. Symposium on Earth Reinforcement, ASCE. (1978).

[41] Moradi, G. Seismic Response Analysis of Geosynthetic Reinforced Soil Retaining Wall. Electronic Journal of Geotechnical Engineering, 19, 3819-3835(2014)

[42] Murthy, V.N.S. Geotechnical engineering: principles and practices of soil mechanics and foundation engineering. Marcel Dekker, Inc., New York (2003)